Direct numerical simulation of passive scalar in decaying compressible turbulence

Xinliang Li [1],Dexun Fu [2],YanwenMa[2]
1 .LNM, Institute of Mechanics, CAS, Beijing China. Email: lixl@lnm.imech.ac.cn
2.LNM, Institute of Mechanics, CAS, Beijing, China. Email: fudx@lnm.imech.ac.cn.

Corresponding author: Xinlang Li

Abstract :

The passive scalars in the decaying compressible turbulence with the initial Reynolds number (defined by Taylor scale and RMS velocity) Re=72, the initial turbulent Mach numbers (defined by RMS velocity and mean sound speed)[2,3] Mt=0.2-0.9, and the Schmidt numbers of passive scalar Sc=2-10 are numerically simulated by using a 7th order upwind difference scheme and 8th order group velocity control scheme. The computed results are validated with different numerical methods and different mesh sizes. The Batchelor scaling with k^{-1} range is found in scalar spectra. The passive scalar spectra decay faster with increasing the turbulent Mach number. The sheet-like structures of the passive scalar gradient are also founded. The extended self-similarity (ESS) is found in the passive scalar of compressible turbulence.

Keyword: *passive scalar, decaying compressible turbulence, direct numerical simulation*

1. Introduction

Direct Numerical Simulation (DNS) becomes an important tool in recent research of turbulence. DNS of compressible turbulence is more difficult than that of the incompressible turbulence. When the turbulent Mach number is greater than 0.3 the shocklets may appear in the compressible turbulent flow fields. The reason and mechanism of shocklets existence is not clear yet. The turbulent Mach number in DNS can not be very high with the present existing numerical methods and computer resource. For the problem of compressible isotropic turbulence with the initial Reynolds number Re= 72 (based on Taylor scale and RMS velocity), as the initial turbulent Mach number is less than 0.5, the tenth order accurate symmetrical compact difference method in Ref [2] can work, but as the turbulent Mach number is greater than 0.5, this method is not valid.

The same problems but with much higher turbulent Mach numbers Mt=0.7 and 0.95 are solved by authors of this paper with high-order upwind difference scheme and GVC8 scheme[3,4].

There are many problems related with the scalar flux in turbulence, such as the pollutant density in the air, chemical or biological species concentration and salinity in the ocean, et al. Since 1990s, many works with DNS have been done in studying the passive scalars of turbulent flow. In recent years some results of DNS for passive scalars with relative high Schmidt number (Sc > 1) are reported [5-8]. All those DNS results of passive scalars are for the incompressible turbulent flows, but the scalars in compressible turbulent flows is more interested in aeronautics and astronautics, for example, the mixing of fuel and air in supersonic ramjet is a typical problem of scalars in compressible turbulent flow.

In this paper the passive scalars in decaying compressible turbulence are solved with direct numerical simulation by using 7th order accuracy upwind difference scheme and 8th order accuracy group velocity control (GVC8) scheme. The start Reynolds number Re= 72, the turbulent Mach numbers Ma=0.2-0.9, and the Schmidt numbers of passive scalars Sc=2-10 are used in computation. In order to validate the computed results, the numerical experiments are made with different simulation methods but with same fluid parameters. In order to check if the small structures we are interested in are captured, the same problems are solved with mesh doubling. Numerical experiments show that the results given in this paper are reliable. The Batchelor k^{-1} range in scalar spectrum is found in our simulations. The effect of compressibility on the flow structures is discussed. The results show that the high wave number spectrum decays faster with increasing the turbulent Mach number. From our

Report Documentation Page

Form Approved
OMB No. 0704-0188

1. REPORT DATE	2. REPORT TYPE	3. DATES COVERED
14 APR 2005	**N/A**	**-**

4. TITLE AND SUBTITLE	5a. CONTRACT NUMBER
Direct numerical simulation of passive scalar in decaying compressible turbulence	5b. GRANT NUMBER
	5c. PROGRAM ELEMENT NUMBER
6. AUTHOR(S)	5d. PROJECT NUMBER
	5e. TASK NUMBER
	5f. WORK UNIT NUMBER
7. PERFORMING ORGANIZATION NAME(S) AND ADDRESS(ES) **LNM, Institute of Mechanics, CAS, Beijing China**	8. PERFORMING ORGANIZATION REPORT NUMBER
9. SPONSORING/MONITORING AGENCY NAME(S) AND ADDRESS(ES)	10. SPONSOR/MONITOR'S ACRONYM(S)
	11. SPONSOR/MONITOR'S REPORT NUMBER(S)

12. DISTRIBUTION/AVAILABILITY STATEMENT
Approved for public release, distribution unlimited

13. SUPPLEMENTARY NOTES
See also ADM001800, Asian Computational Fluid Dynamics Conference (5th) Held in Busan, Korea on October 27-30, 2003. , The original document contains color images.

14. ABSTRACT

15. SUBJECT TERMS

16. SECURITY CLASSIFICATION OF:			17. LIMITATION OF ABSTRACT	18. NUMBER OF PAGES	19a. NAME OF RESPONSIBLE PERSON
a. REPORT **unclassified**	b. ABSTRACT **unclassified**	c. THIS PAGE **unclassified**	**UU**	**8**	

computed results it is found that in the compressible turbulence there is also the extended self-similarity (ESS) for the passive scalars.

The methods used in the computation are presented in section 2, the validation of results is given in section 3, and the computed results are analyzed in section 4.

2 Numerical method

The compressible Navier-Stocks equations are written in the vector form as follows

$$\frac{\partial \mathbf{U}}{\partial t}+\frac{\partial \mathbf{E}}{\partial x}+\frac{\partial \mathbf{F}}{\partial y}+\frac{\partial \mathbf{G}}{\partial z}=\frac{\partial \mathbf{E}_v}{\partial x}+\frac{\partial \mathbf{F}_v}{\partial y}+\frac{\partial \mathbf{G}_v}{\partial z}\ , \qquad (1)$$

and the transport equation for the passive scalar expressed as

$$\frac{\partial(\rho g)}{\partial t}+\frac{\partial(\rho u g)}{\partial x}+\frac{\partial(\rho v g)}{\partial y}+\frac{\partial(\rho w g)}{\partial z}=\frac{1}{Re\,\mathrm{Sc}}\left(\frac{\partial}{\partial x}\left(\mu\frac{\partial g}{\partial x}\right)+\frac{\partial}{\partial y}\left(\mu\frac{\partial g}{\partial y}\right)+\frac{\partial}{\partial z}\left(\mu\frac{\partial g}{\partial z}\right)\right) \qquad (2)$$

where $\mathbf{U}=[\rho,\rho u,\rho v,\rho w,e]^T$, $\mathbf{E},\mathbf{F},\mathbf{G},\mathbf{E}_v,\mathbf{F}_v,\mathbf{G}_v$ are the convection terms and the viscous terms[9], respectively. The viscosity coefficient μ is obtained from the Sutherland equation, g is the passive function, and Sc is the Schmidt number.

Periodic boundary conditions and uniform meshes are used in x-, y- and z- directions. The initial conditions of the velocity components, the pressure and the temperature are given as in Ref. [3], and the initial condition for the passive scalar is given in the same way as that of u component of the velocity vector.

The viscous terms of the Navier-Stokes equations are discretized with 8th order center difference. The flux vector splitting is adopted for the convection terms. The 7th order accurate upwind difference approximation in Ref.[3] and the GVC8 in Ref.[4] are used to discretized the convection terms.

Consider the approximation for the first derivative in the convection terms

$$u'_j=(F_{j+1/2}-F_{j-1/2})/\Delta$$

For the positive flux the following backward difference approximation is used

$$F_{j+1/2}=\sum_{k=1}^{9} b_k u_{j+5-k}$$

$$b_k=\begin{cases} b_k^{(1)} & when \quad \left|\Delta u_{j-1/2}\right|\le\left|\Delta u_{j+1/2}\right| \\ b_k^{(2)} & when \quad \left|\Delta u_{j-1/2}\right|>\left|\Delta u_{j+1/2}\right| \end{cases}$$

where $\Delta u_j=u_{j+1}-u_{j-1}$

The coefficients $b_k^{(1)}$ and $b_k^{(2)}$ are given in the following table.

Table 1. Values of $b_k^{(1)}$ and $b_k^{(2)}$

k	1	2	3	4	5	6	7	8	9
$b_k^{(1)}$	$\frac{17}{7000}$,	$-\frac{283}{21000}$,	$\frac{53}{21000}$,	$\frac{6269}{21000}$,	$\frac{4429}{4200}$,	$-\frac{10531}{21000}$,	$\frac{4253}{21000}$,	$-\frac{361}{7000}$,	$\frac{3}{500}$
$b_k^{(2)}$	$-\frac{4}{875}$,	$\frac{893}{21000}$,	$-\frac{4063}{21000}$,	$\frac{14501}{21000}$,	$\frac{2371}{4200}$,	$-\frac{2299}{21000}$,	$\frac{137}{21000}$,	$\frac{31}{7000}$,	$-\frac{1}{1000}$

For the negative flux the following forward difference approximation is used:

$$F_{j+1/2}=\sum_{k=1}^{9} a_k u_{j+4-k}$$

where $a_k=\begin{cases} b_{10-k}^{(2)} & when \quad \left|\Delta u_{j-1/2}\right|<\left|\Delta u_{j+1/2}\right| \\ b_{10-k}^{(1)} & when \quad \left|\Delta u_{j-1/2}\right|\ge\left|\Delta u_{j+1/2}\right| \end{cases} \quad (k=1,2\cdots 9)$

The difference approximation for the passive scalar is the same as that for the Navier-Stokes equations. To save computing resource the Reynolds number in computation is not very high, and the grid number for the passive scalar is doubled in each direction comparing with the grid number for other flow parameters. 8th order Langrage interpolation is used to transport the value of coarse mesh to the fine mesh.

The parameters used in the DNS cases are shown in the following table

Table 2. Computing parameters of each DNS cases

CASE	Re_λ	Mt	Sc	Numerical Method	Grid number for fluid	Grid number for passive scalar
D1	72	0.2	5	UD7	256×256×256	512×512×512
D2	72	0.5	5	UD7	256×256×256	512×512×512
D3	72	0.7	5	UD7	256×256×256	512×512×512
D4	72	0.9	5	GVC8	256×256×256	512×512×512
E1	72	0.5	2	UD7	256×256×256	512×512×512
E2	72	0.5	10	UD7	256×256×256	512×512×512
E1T	72	0.5	2	UD7	128×128×128	256×512×512
D2Ta	72	0.5	5	UD7	128×128×128	256×256×256
D2Tb	72	0.5	5	GVC8	256×256×256	512×512×512

In Table 2 Re_λ is the initial Reynolds number, Mt is the initial turbulent Mach number, and Sc is the Schmidt number. UD7 in Table 2 denotes 7th order upwind difference method [3] and GVC8 denotes 8th order group velocity control scheme.

The initial Reynolds number equal to 72 for all cases in computation, the Schmidt number is in the range 2-10, and the initial turbulent Mach number is in the range 0.2-0.9. The flow parameters for the case E1T in Table 2 are the same as for the case E1, and the parameters for D2Ta, D2Tb are the same as for D2. These three cases E1T, D2Ta and D2Tb are used to validate numerical results.

Programs are coded by using MPI Fortran 77, and the DNS results are computed with the LSSC2 computer of LSEC (State Key Laboratory of Scientific and Engineering Computing). Averaged performance are: 11 seconds/time-step for case E1T and D2Ta (8 CPUs in 8 nodes), 18.6 seconds/time-step for cases D1-D3 and E1-E2 (64 CPUs in 32 nodes), 20.5 seconds/time-step for case D4 and D2Tb (64 CPUs in 32 nodes).

3. Validation of computed results

3.1 The flow parameters

All the flow parameters obtained from numerical simulations have been validated by the authors in papers [3-4].

In Fig.1 is shown the time history of normalized average kinetic energy $K(t)/K_0$ and velocity derivative skewness for Case D2. Horizontal ordinate in Fig.1 denotes the normalized time t/τ. Where $\tau = \sqrt{\frac{32}{A}}(2\pi)^{1/4} k_0^{-7/2}$ is the large-eddy-turnover time at t=0 [2]. The symbols in this figure are the results given in Ref.[2] by using 10th order accurate Pade schemes with the same computing parameters, including the initial Reynolds number and initial turbulent Mach number, as these in Case D2. Fig.1 shows that the results of this paper agree well with the results of Ref. [2], and this validated our results of flow fields.

The numerical experiments for the case with Reynolds number Re_λ=72 show that the grid number 128×128×128 is enough for obtaining the accurate results. In this paper, the gird systems 128 ×128×128 and 256×256×256 are used for simulating the flow field parameters.

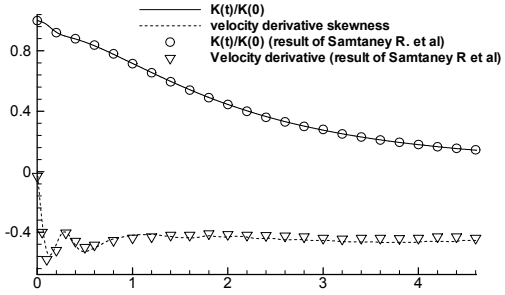

Figure 1. Time history of normalized kinetic energy and velocity derivative skewness for case D2 and the results of Samtaney et al.

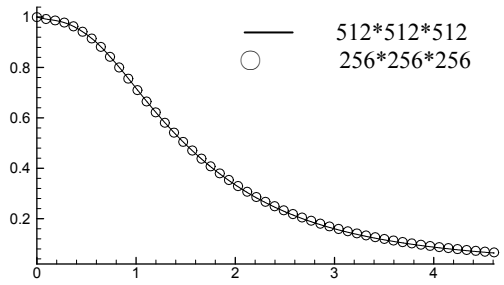

Figure 2. Time history of RMS passive scalars for case E1 (512*512*512) and E1T (256*256*256)

3.2 The passive scalars

We will compare the statistics of passive scalars in each DNS cases by using different numerical methods and with different grid sizes. Numerical experiments show that the statistics is not sensitive with different numerical methods or grid size if the grid number is large enough (more than or equal to 128×128×128). This means that the small structures we are interested in are captured.

Figure 2 shows the time history of RMS passive scalars for Case E1 and E1T. The computing parameters and numerical method are the same for these two cases, but the grid number are 512×512 ×512 and 256×256×256 for these two case respectively. The RMS of passive scalar is defined as: $R_g(t) = g_{rms}(t)/g_{rms}(0)$, $g_{rms} = \sqrt{< g^2 >}$. From fig.2 we can see that the two results agree well with each other. In Fig. 3 is shown the time history of RMS passive scalar for case D2 and D2Ta, from which we also can see that grid size is small enough for simulating physical phenomena we are interested in. This experiment tells us that the error due to grid size is negligible.

Fig.4 shows the time history of RMS passive scalar for case D2 and D2Tb. The flow parameters and the grid numbers in computation for these two cases are the same, but the numerical methods are different. The 7^{th} order upwind difference scheme is used for the case D2, and GVC8 scheme is used for the case D2Tb. From this figure we can see that the results of these two cases agree well with each other. This numerical experiment also validate our numerical results.

As it is known that the grid number in each direction needs to be the magnitude of $Pe^{3/4}$ where $Pe = Re \times Sc$ is the Pe number. We can infer that the grid number for the case D4 is enough because the Pe number for case D4 is the same as for the case D1-D3. We can also infer that the grid number for E2 is sufficient because the grid number for E2 is doubled comparing with the case D2Ta in each direction. This grid number is more than the needed.

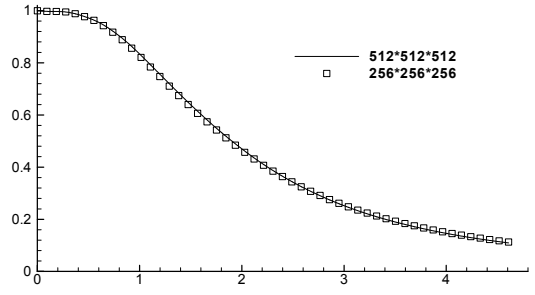

Figure 3. Time history of RMS passive scalar for case D2 (512*512*512) and D2Ta (256*256*256)

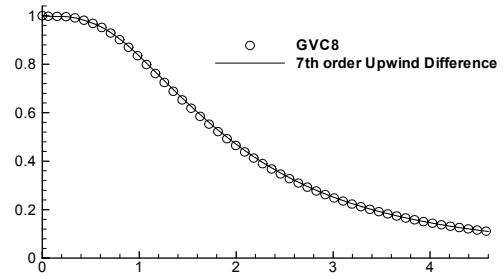

Figure 4. Time history of RMS passive scalar for case D2 (GVC8 scheme) and D2Tb (7^{th} order upwind difference scheme)

4. Analysis of Numerical Results

We will study the flow field and passive scalar field for each DNS case at $t/\tau = 1$. The parameters of these fields are showed in the following table. Turbulence after $t/\tau = 0.8$ may be considered realistic [2,3]. The results obtained at $t/\tau = 1$ are analyzed.

Table 3. The parameters of the flows and passive scalar fields

Field Number	DNS CASE	t/τ	Re_λ	Mt	Sc	S_u	S_{ug}
FD1	D1	1.0	39.4	0.17	5	-0.44	-0.63
FD2	D2	1.0	38.5	0.42	5	-0.40	-0.63
FD3	D3	1.0	36.3	0.42	5	-0.42	-0.51
FD4	D4	1.0	33.4	0.72	5	-0.69	-0.57
FE1	E1	1.0	38.5	0.42	2	-0.40	-0.64
FE2	E2	1.0	38.5	0.42	10	-0.40	-0.62

where $S_u = \dfrac{<u^3>}{<u^2>^{3/2}}$, $S_{ug} = \dfrac{<u^2 g>}{<u^2><g^2>^{1/2}}$。

4.1 Spectral analysis of passive scalar

Batchelor (1959) found that there is k^{-1} range in the energy spectrum of passive scalar when the Schmidt number is much large than 1. In later researches it was found that "k^{-1} range" in the spectrum exists only when the Schmidt number large than 1 (need not much large than 1). But in some experiments "k^{-1} range" for the passive scalar spectrum has not been found yet [6]. In all these research works the passive scalars are discussed only for the incompressible turbulence, and the effects of compressibility on passive scalars are still unknown.

The energy spectrum of passive scalar is defined as:

$$E_g(k) = 4\pi k^2 \left\langle \hat{g}(k_1,k_2,k_3)\hat{g}^*(k_1,k_2,k_3) \right\rangle_k$$

where $\hat{g}$ is the spectrum of g, $\hat{g}^*$ is the conjugate of $\hat{g}$. The shell average of spectrum at the range $[k-1/2, k+1/2)$ is expressed as

$$\left\langle f(k_1,k_2,k_3) \right\rangle_k = \frac{1}{N_k} \sum_{k-1/2 \le \tilde{k} < k+1/2} f(k_1,k_2,k_3)$$

where $k = \sqrt{k_1^2 + k_2^2 + k_3^2}$.

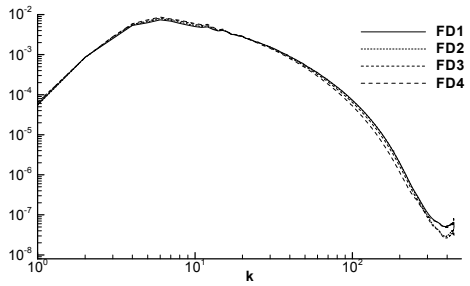

Figure 5. Energy spectrum of passive scalar for FD1-FD4

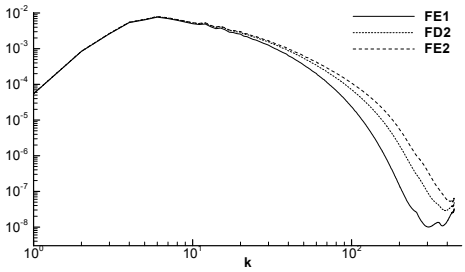

Figure 6. Energy spectrum of passive scalar for FE1, FD2 and FE2

Fig.5 shows the energy spectrum of passive scalar E_g for FD1-FD4 (scalar fields at $t/\tau = 1$ of cases D1-D4). We can find that the spectrum decays faster in the range of high wave number with turbulent Mach number increasing. This is because that more kinetic energy will be dissipated by shocklets with turbulent Mach number increasing.

Fig.6 shows the energy spectrums of passive scalars for the cases FE1, FD2 and FE2. The Schmidt number for these three cases is 2, 5 and 10 respectively. This figure shows that the energy

spectrum of passive scalar decays slower with the increasing Schmidt number. The amplitude of the highest wave number of the spectrum is about 10^{-8} which shows the sufficient accuracy of our simulations.

Fig.7 shows the normalized energy spectrum of passive scalars for cases FE1 FD2 and FE2. The horizontal ordinate is $k\eta_B$ and the vertical ordinate is $(k\eta_B)E_g/(\chi(\upsilon/\varepsilon)^{1/2}\eta_B)$ where η_B is Batcher scale, ε and χ is the dissipate rate of kinetic and passive scalar respectively. The normalized energy spectrum $(k\eta_B)E_g/(\chi(\nu/\varepsilon)^{1/2}\eta_B)$ remains unchanging in a relative long interval. This result means that exists relation $E_g \sim k^{-1}$ in this interval, and this Batchelor k^{-1} spectral is universal for all these cases considered.

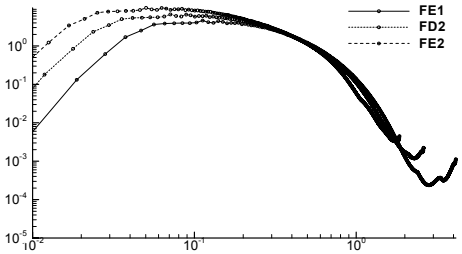

Figure 7. Normalized energy spectrum of passive scalar of FE1, FD2 and FE2.

4.2 Coherent structure of passive scalar in compressible isotropic turbulence

The sheet-like structures in passive scalar in incompressible turbulence are reports in some recent research works, but there still no reports about coherent structures of passive scalar in compressible turbulence.

Let $\theta = \frac{1}{\theta_{rms}}\sqrt{(\frac{\partial g}{\partial x})^2+(\frac{\partial g}{\partial y})^2+(\frac{\partial g}{\partial z})^2}$, where θ_{rms} is the root-mean-square of the scalar gradient $\sqrt{(\frac{\partial g}{\partial x})^2+(\frac{\partial g}{\partial y})^2+(\frac{\partial g}{\partial z})^2}$

Figure 8 and Figure 9 shows the isosurface of $\theta = 2$ for FD2 and FD4, respectively. The visualizing domain is the 1/64 of the full computing domain. The two figures show the sheet structure of passive scalar in compressible turbulence.

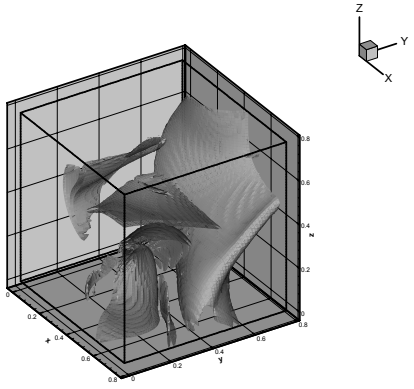

Figure 8. Isosurface of normalized scalar gradient of FD2

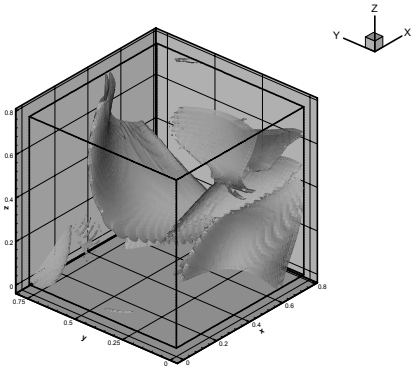

Figure 9. Isosurface of normalized scalar gradient of FD4

4.3 Scaling analysis of passive scalar in compressible isotropic turbulence

Scaling law is a hot topic in turbulence physics in recent years. Extended self-similarity (ESS) is one of the important developments in measurement of the scaling exponents. She et al developed S-L model of scaling law, which has been tested by several experiments and numerical dates. The scaling law of the passive scalar in turbulent flow has been reported in recent years. Zhou et al[8] studied the scaling law of passive scalar for the incompressible isotropic turbulence. But there is still no report for scaling law of passive scalar for the compressible turbulence.

Fig. 10 are given the plots of p-th order passive scalar structure functions as function of 3rd order passive scalar structure function for the case FD2. The horizontal ordinate is $\log <|\delta g_l|^3>$, and the vertical ordinate is $\log <|\delta g_l|^p>$ where $\delta g_l = g(x+l) - g(x)$, and $\langle\cdot\rangle$ denotes the average over the all field. From the plot we can see clearly the linear variation, which means that the power laws between p-th order passive scalar structure function and 3rd order passive scalar structure function. This means ESS (Extended Self-Similarity) holds in the compressible passive scalar turbulence.

Fig.11 and Fig.12 are shown the same plots for the passive scalar field for the case FD4 and FE2, respectively. From these two figures we can obtain the same conclusion as that in figure 10. The rates of slope in the plots in fig. 10-12 are the relative scalar exponent ζ_p, and the least square approximate method is used to calculate these slope rates.

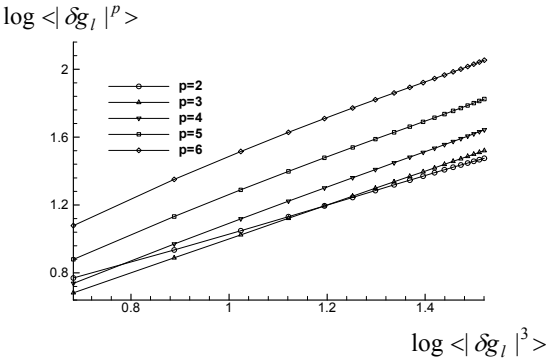

Figure 10. Plots of p-th order passive structure functions as functions of 3rd passive structure in FD2

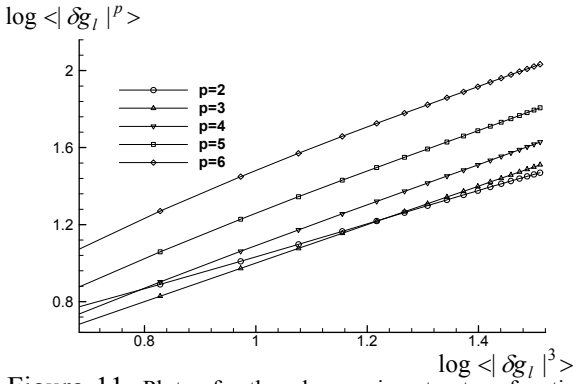

Figure 11. Plots of p-th order passive structure functions as functions of 3rd passive structure in FD4

Fig. 13 shows the relative scaling exponents for the cases FD1-FD4. The dash line denotes p/3 law. The exponents lower than p/3 denote the strong intermittence of the passive scalar field. This figure indicates that the compressibility has little effect on passive scalar's scaling exponents, for example, the largest difference of ζ_6 is not more than 4% and the largest difference of ζ_7 is not more than 5% among the four cases.

Fig.14 shows the relative scaling exponents for FE1, FD1 and FE2 with Schmidt numbers 2, 5 and 10 respectively. This figure shows scaling exponent become smaller with increasing Schmidt number. It means that the passive scalar become more intermittent with the increasing Schmidt number.

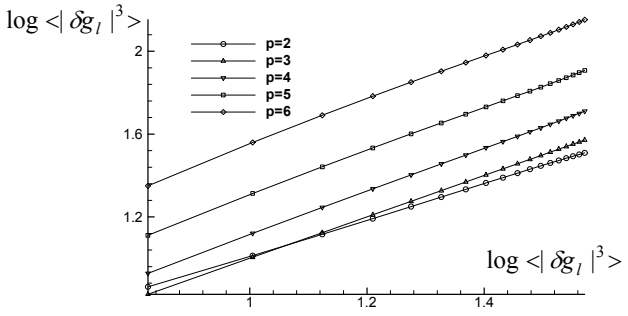

Figure 12. Plots of p-th order passive structure functions as functions of 3rd passive structure in FE2

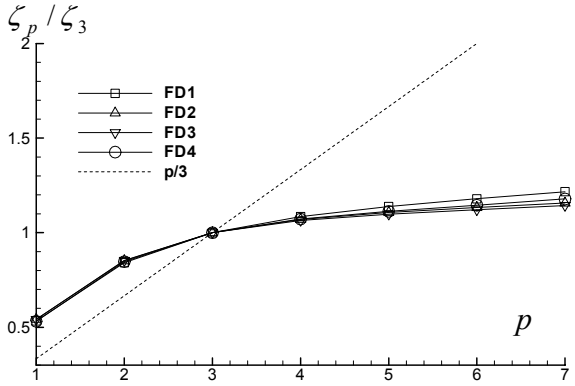

Figure 13. Relative scaling exponents of passive scalar for FD1-FD4

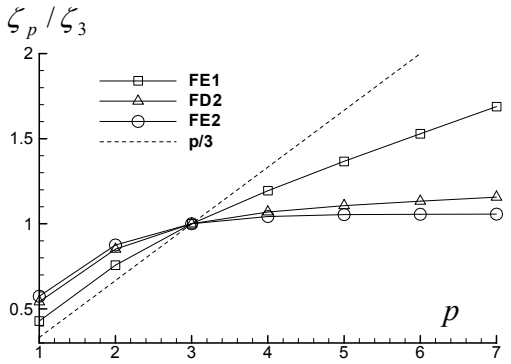

Figure 14. Relative scaling exponents of passive scalar for FE1, FD2 and FE2

5. Conclusion

1. There is clear Batchelor k^{-1} range in the energy spectrum of passive scalar in the compressible turbulent flow, and the compressibility effect leads to faster decay of energy spectrum of passive scalar in high wave number ranges.
2. The sheet-like structures of the passive scalar gradient are founded in compressible isotropic turbulence.
3. The ESS holds in the passive scalar of compressible turbulence, and the compressibility has little effects on the relative scalar exponents of passive scalar.
4. The exponents of passive scalar became more intermittent with Schmidt number increasing.

Acknowledgements: The authors would like to thank the State Key Laboratory of Scientific and Engineering Computing (LSEC) for providing computer time. The authors thank Professor Zhang Linbo of LSEC for the help in programming, and thank Professors He Guowei for the help in settling initial condition of the DNS.

Reference

[1] Moin P, Mahesh K. Direct Numerical Simulation: A Tool in Turbulence Research. Annu. Rev. Fluid Mech. 1998.30:535-78

[2] Samtaney R, Pullin D I, Kosovic B. Direct numerical simulation of decaying compressible turbulence and shocklet statistics. Phys. Fluids, 2001,13(5),1415-1430

[3] Li X L, Fu D X, Ma Y W. Direct numerical simulation of compressible isotropic turbulence. Science in China A, 45(11), 2002, 1452-1460.

[4] Li X L, Fu D X, Ma Yanwen. Direct numerical simulation of decaying compressible turbulence (in Chiniese). Poceedings of the 11th Conference on Computational Fluid Dynamics, 2002, 123－128

[5] Yeung P K, Sykes M C, Vedula P. Direct numerical simulation of differential diffusion with Schmidt number up to 4.0. Physics of Fluids, 2000,12(6), 1601-1604

[6] Bogucki D, Domaradzki J A, Yeung P K. Direct numerical simulations of passive scalars with Pr>1 advected by turbulent flow. J. Fluid Mech. 1997, 343,111-130

[7] Zhou H B, Cui G X, Xu C X, Zhang Z S. Thin layer structure of dissipation rate of scalar turbulence, Science in China, Series E. 2003, 46 (2), 209-217

[8] Zhou H B, Cui G X, Zhang Z S. et al. Dependence of turbulent scalar flux on molecular Prandtl number. Physics of Fluids,2002,14(7), 2388-2394

[9] Fu D X, Computational aerodynamics (in Chinese). 1994, Astronavigation Publishing Company.

[10] Benzi R, Ciliberto S, Tripiccione R, et al. Extended self-similarity in turbulence flows. Phys. Rev. E, 1993,48(1),29-32